Int. J. Multiphase Flow Vol. 17, No. 1, pp. 27–44, 1991
Printed in Great Britain

0301-9322/91 $3.00 + 0.00
Pergamon Press/Elsevier

FLOODING AND CHURN FLOW IN VERTICAL PIPES

A. H. GOVAN, G. F. HEWITT, H. J. RICHTER† and A. SCOTT‡
Thermal Hydraulics Division, Harwell Laboratory, Oxon. OX11 0RA, England

(Received 8 December 1989; in revised form 26 September 1990)

Abstract—Experimental studies are reported on the flooding phenomenon and on the closely associated churn flow regime. Flooding experiments were carried out with air–water flow in a 32 mm dia vertical pipe with various forms of liquid outlet, namely a porous wall, a tapered outlet and a square-edged outlet. For the first time, downflow (penetration) measurements were made with the porous wall outlet and showed significant differences between penetration rates beyond flooding and the flooding rate. This contrasts with other types of injectors, where the mechanisms of flooding are somewhat different. Measurement of pressure drop and holdup in the churn flow regime were made both with and without a co-existing falling film below the liquid injector. These showed that the falling-film and churn flow regions were essentially decoupled. Analysis of the data for churn flow showed that the minimum pressure gradient does not, for this data, correspond to the condition of zero wall shear stress as had been suggested by some earlier analytical studies. Interfacial shear stresses in churn flow were compared with those used in current reactor safety codes (TRAC and RELAP) and it was found that, for the churn flow region, the relationships used in the RELAP code were more appropriate.

Key Words: gas–liquid flow, churn flow, annular flow, flooding, pressure drop, holdup, vertical flow.

1. INTRODUCTION

An important class of counter-current two-phase flow is that of falling-film flow, in which a gas flows upwards, counter-current to a liquid film on the channel walls, falling under gravity. Such flows occur in many practical situations such as falling-film evaporators and emergency-cooling of a nuclear reactor. There is considerable interest in the phenomenon of "flooding", which represents a limit to the pure counter-current flow region. Here, we shall define flooding as the condition at which liquid begins to be carried upwards above the liquid injector, this condition being approached by increasing either or both of the phase flowrates. Beyond the flooding point, part of the liquid flows upwards above the injector and part may flow downwards. The downflow region is one of counter-current flow whereas, above the injector, a highly disturbed region of co-current flow occurs which we shall refer to as "churn flow". Though the net upwards flow of the liquid in the churn flow regime is zero or positive, the flow can vary transiently in direction as shown by Hewitt *et al.* (1985).

There have been a very large number of published studies of flooding, but in spite of this, there is still confusion over the mechanisms involved and many of the data and correlations are in poor agreement. This diversity in the data can be illustrated by comparing it with one of the most widely used correlations for the onset of flooding, namely that of Wallis (1961). This correlation is as follows:

$$U_G^{*1/2} + U_L^{*1/2} = C, \qquad [1]$$

where C is a constant whose value Wallis suggested should be around unity. U_G^* and U_L^* are defined as

$$U_G^* = U_G\left[\frac{\rho_G}{gd(\rho_L - \rho_G)}\right]^{1/2} \qquad [2]$$

and

$$U_L^* = U_L\left[\frac{\rho_L}{gd(\rho_L - \rho_G)}\right]^{1/2}, \qquad [3]$$

†On attachment from Dartmouth College, Hanover, NH 03755, U.S.A.
‡Vacation student from the Department of Chemical Engineering, Imperial College of Science, Technology and Medicine, London SW7 2BY, England.

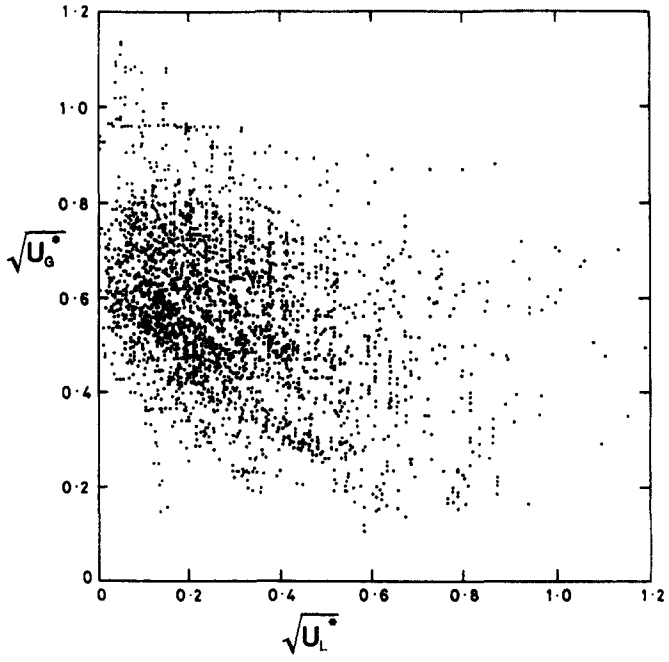

Figure 1. Flooding date [from McQuillan (1985)].

where d is the hydraulic diameter of the channel, U_G and U_L are the gas and liquid superficial velocities, ρ_G and ρ_L are the gas and liquid densities and g is the acceleration due to gravity. Figure 1 [taken from McQuillan (1985)] shows a large range of flooding data, plotted in terms of $U_L^{*1/2}$ and $U_G^{*1/2}$, which illustrates the large scatter which exists.

There are two main reasons for the lack of agreement. Firstly, the onset of flooding appears to be very sensitive to the test-section geometry, particularly the inlet and outlet configurations. Secondly, there has been some inconsistency in the past in the definition of the onset of flooding and of the related phenomena of "deflooding" (i.e. the point at which the pure counter-current flow region is reinstated on *reduction* of flow after flooding) and liquid downflow (or "penetration") rate in the region beyond flooding. Reviews of the literature are given by Bankoff & Lee (1986) and Hewitt (1989). The available data suggests that the geometry of the liquid outlet has a very large influence on the onset of flooding. Of the wide range of possible geometries illustrated in Bankoff & Lee's (1986) review, the three principal types used by experimenters are as shown in figure 2: (a) a porous wall outlet; (b) and (c) tapered (or bell-mouth) outlets; (d) and (e) square-edged outlets. Several published studies (e.g. Feind 1960; Hewitt 1977) have suggested that the flooding curve (U_G vs U_L) for (a) lies above that for (b) and (c), which in turn lie above that for (d) and (e). Furthermore, the studies of Hewitt *et al.* (1965) and McQuillan (1985) using outlet

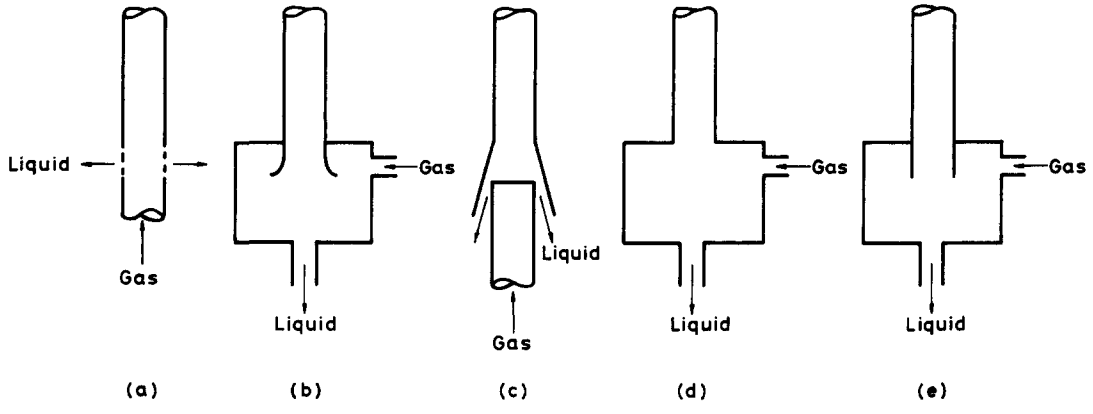

Figure 2. Principal types of liquid outlet geometry used in flooding studies.

type (a), have shown a strong influence of the length of the falling-film region on the flooding curve while others, such as Zabaras & Dukler (1988), using outlet type (b) show no effect of length.

The work described in this paper aims to throw further light on flooding and the associated phenomena of deflooding, churn flow and penetration. The main objectives were as follows:

(A) To carry out a series of flooding measurements *in the same apparatus* to give direct comparison between the data for porous wall, square-edged and bell-mouth outlets, making detailed visual observations in each case to elucidate the governing phenomena.

(B) To measure the downflow rate beyond flooding. Zabaras & Dukler (1988) found that the flooding and downflow rates were equal. For smooth, porous wall outlets, this is not the case. To the authors' knowledge, measurements of liquid downflow rates beyond flooding have not been made previously with smooth outlet conditions and the new measurements, reported here, allow the overall picture to be clarified.

(C) To make specific measurements of pressure gradient and liquid holdup in churn flow, the churn flow investigated being set up in two ways

  (i) By increasing flows beyond flooding in a flooding experiment and making measurements above the liquid entry point. In this case, there exists a counter-current flow region below the injector.

  (ii) By introducing both phases at the bottom of the tube and setting conditions such that churn flow exists over the whole tube. In this case there is no co-existing churn flow region.

By comparing (i) and (ii) it was possible to establish that, beyond flooding, the falling-film and churn flow regions were essentially decoupled. Furthermore, the new data on churn flow (for which there is actually a dearth of previous data) could be analysed to throw new light on the pressure drop minimum phenomenon.

2. EXPERIMENTS ON FLOODING

2.1. Apparatus and Test Sections

The experiments were carried out on a low-pressure air–water facility at Harwell which supplied filtered, metered air to the test section. Air flow measurement was by means of a standard orifice plate and water flow measurements by means of calibrated rotameters. The air pressure at the test section outlet was maintained at 1.33 bar for all the experiments and the fluid temperatures were close to ambient (namely 20°C). The air passing from the apparatus was separated from any liquid passing out with it in a cyclone separator and was discharged to the atmosphere. The water was returned to a sump tank. The following two types of test section were employed.

2.1.1. Porous wall outlet

The test section (figure 3) is comprised of flanged lengths of 31.8 mm i.d. acrylic resin or drawn copper tubing. The liquid phase enters *via* the upper porous wall section ("inlet sinter") and, before flooding, leaves *via* the lower porous wall section ("outlet sinter"). Beyond flooding some of the liquid phase flows above the injection point into the upper region of the tube. Experiments on this latter region are described in section 3 (on churn flow) below. One of these experiments was to determine the liquid holdup, hence the simultaneously-closing valves in the upper section. The sections below the lower of the two simultaneously-closing valves are of acrylic resin, while the upper sections are of copper. The air enters the test section through a short section of dia 10 mm (to prevent water drainage) which is followed by a 1 m calming length preceeding the liquid outlet sinter. Water is fed to the upper of the two sintered bronze porous wall sections which is 50 mm long. The falling film is removed, together with a small quantity of air, at the lower sinter section (75 mm long) which is positioned at 1.0 or 0.3 m below the inlet sinter. The two-phase flow removed at the sinter is separated in a cyclone; the air flowrate is measured using a gas meter while the water flowrate is measured by timing the rise in the water level in the cyclone. The valve V1 was used

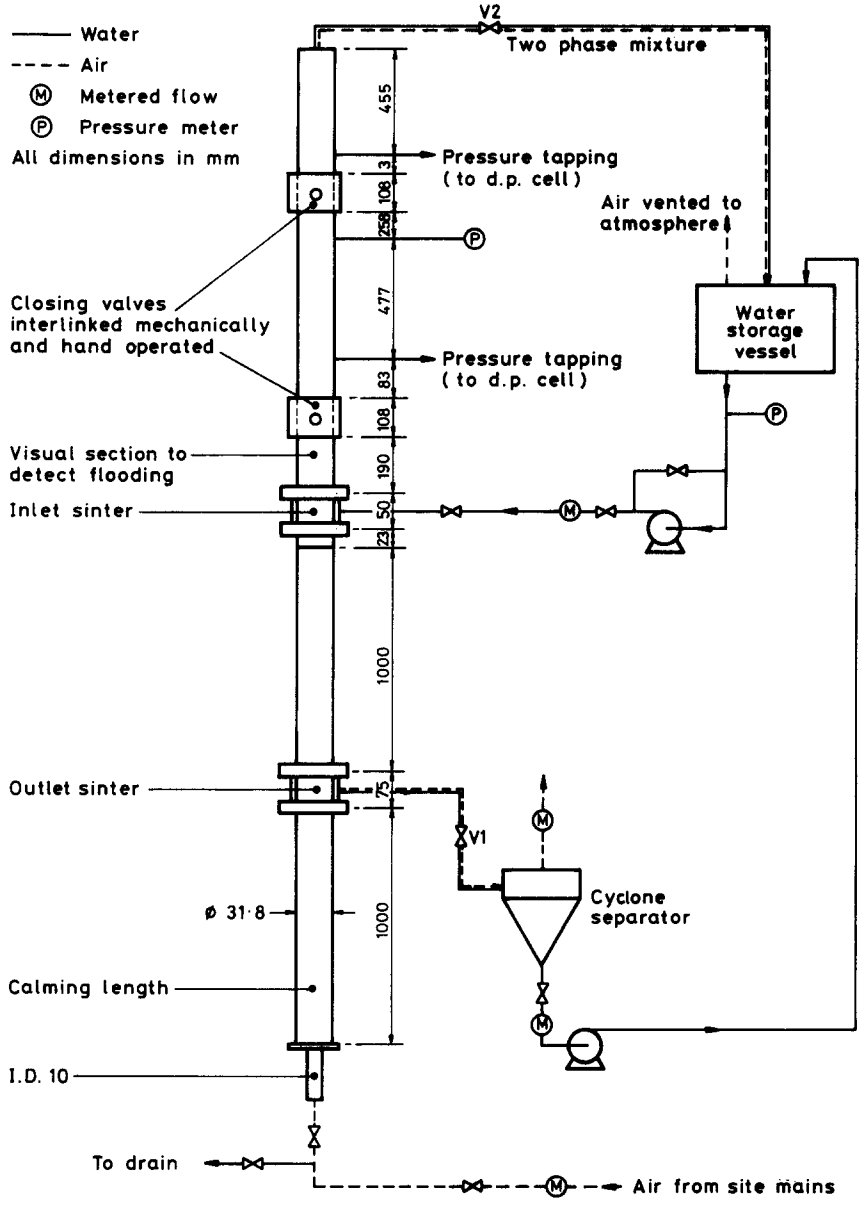

Figure 3. Experimental arrangements with a porous wall outlet.

to minimize the air removal; in the present experiments the air removal varied from 0 (at high gas/low liquid flowrates) to 20% of the air input (at high liquid rates). Typically, the air removed was around 5% of the air input and this was subtracted from the measured air input before carrying out any further analysis. In some of the later experiments a second outlet sinter section (75 mm long) was placed immediately below the first to improve the film removal at high liquid inputs. In all the experiments the pressure at point P was maintained at 1.33 bar using valve V2.

2.1.2. Square-edged and tapered liquid outlets

The apparatus is shown in figure 4; the upper part of the test section is identical to that for the porous wall liquid outlet but the lower sinter section and the air calming length are replaced by a transparent cylindrical vessel which the air enters through a 25 mm pipe. The square-edged outlet is formed by the top plate of this vessel, while the tapered outlet consists of a polycarbonate insert positioned between the pipe flange and the top plate. The geometry of the tapered outlet has the same proportions as that used by Zabaras & Dukler (1988) but the tube diameter was 50 mm in their experiments.

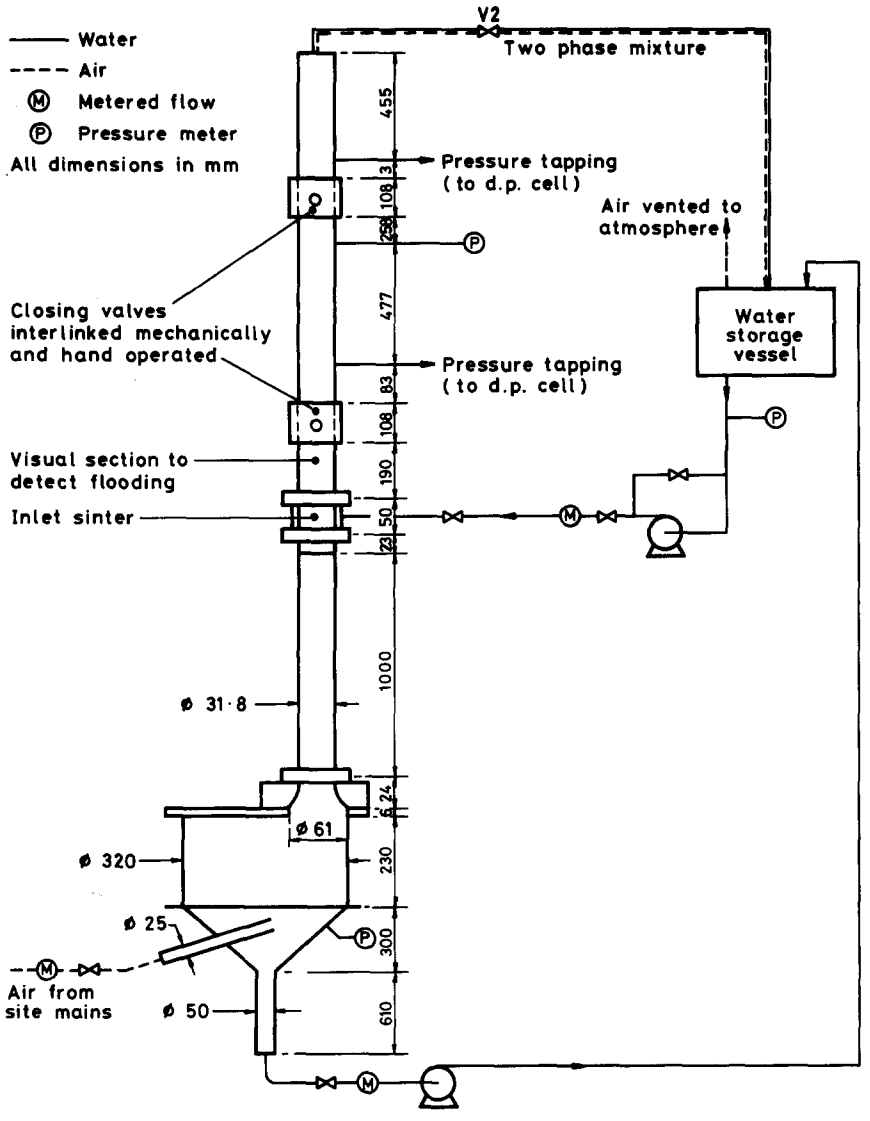

Figure 4. Experimental arrangement with a tapered outlet.

2.2. *Observations and Data*

2.2.1. *Porous wall outlet*

The experimental procedure was to set the water flowrate at a constant value in the range 3–63 g/s, with the air flow initially at a low value so that a falling film is created. The air flow was then gradually increased, maintaining a constant test-section pressure and water flowrate, until flooding was observed. At water flowrates above about 12 g/s flooding occurred suddenly due to the formation of a single wave near the outlet sinter, which travelled rapidly upwards beyond the liquid injection point. At the lowest water flowrates, on the other hand, the transition was more gradual. Small intermittent waves were observed travelling upwards on the falling film but initially these did not travel beyond the liquid injection point. With further increases in the gas velocity, splashing occurs above the liquid injection, and flooding was recorded as the point at which the liquid appeared to travel above the transparent section above the inlet sinter. The gas flow is then increased still further and a series of measurements are made of the liquid downflow rate at various gas flowrates with the test section pressure still maintained at 1.33 bar. The "deflooding" point was measured by gradually reducing the air flow until all the liquid flowed downwards from the injection point. At the higher liquid flows it was necessary to decrease the air flow very slowly because it often took several minutes for the liquid flow distribution to settle down.

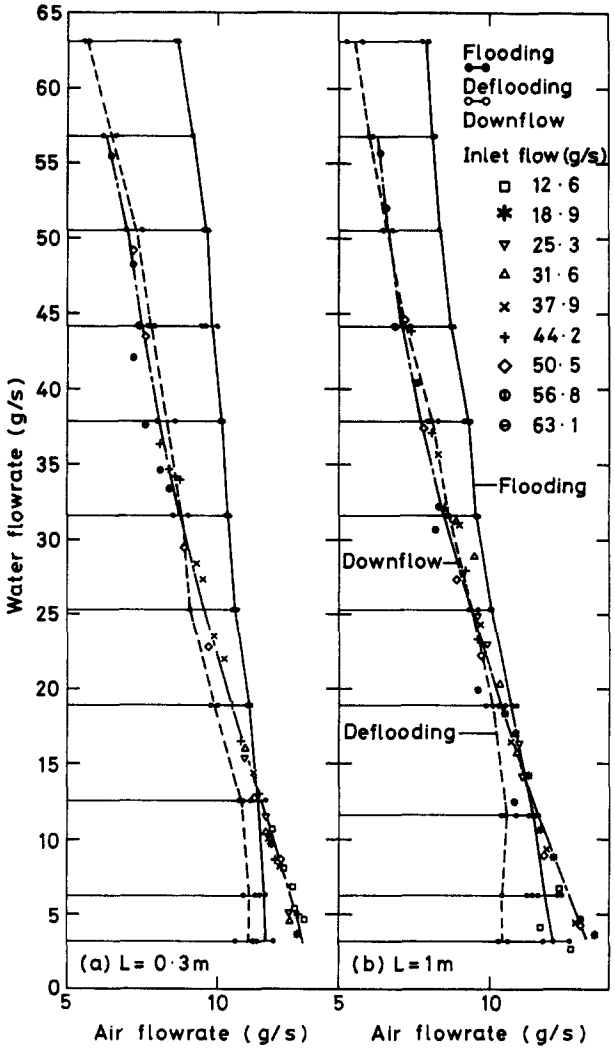

Figure 5. Flooding, deflooding and downflow with a porous wall outlet.

The results are shown in figure 5 for falling-film lengths (i.e. distance between inlet and outlet porous wall sections) of 0.3 and 1.0 m, respectively. For each liquid input flowrate. at least two measurements were made of the flooding and deflooding transitions. To clarify the trends, curves have been drawn through the data showing the flooding and deflooding transitions and the liquid downflow (penetration) rates. The following main points emerge from the results shown in figure 5:

(1) Reproducible data are obtained for flooding and the flooding velocity decreases with increasing length. This latter effect is consistent with the data obtained previously with the same kind of geometry (Hewitt *et al.* 1965; McQuillan 1985). The present results are compared with the previous data in terms of U_G^* and U_L^* [2] and [3] in figure 6. The trends are reasonably consistent; the present results show a somewhat weaker length effect. These results may reflect small differences in the way the experiments were performed, reflecting the sensitivity of the basic phenomenon, as will be discussed in section 2.3 below.

(2) The net results for the residual downflow rate beyond flooding show that the downflow rate is independent of the length of the falling-film region. Furthermore, beyond flooding, the downflow rate is independent of liquid input rate, any additional liquid being carried upwards in churn flow above the injection point.

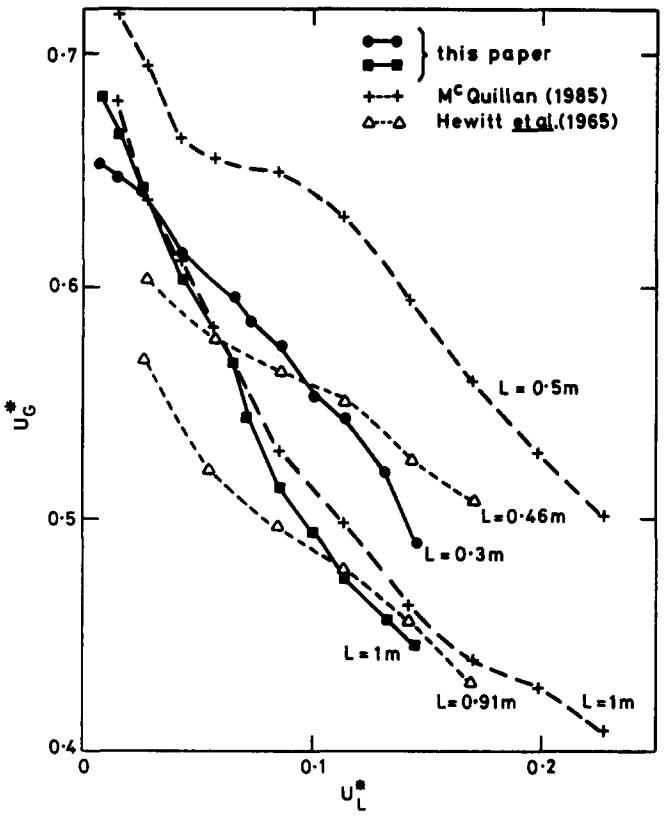

Figure 6. Comparison with the flooding data of Hewitt *et al.* (1965) and McQuillan (1985).

The relationship between the downflow curve and the flooding curve falls into two distinct regions:

(A) At high liquid flowrates, the downflow curve lies well below the flooding curve. Thus, at the flooding point liquid begins to be transported in co-current churn flow out through the air exit of the test section. Note that, in this region, flooding corresponds to the formation of a large wave near the bottom of the test section which is then transported up beyond the liquid injection point. The formation of such large waves is probably essential to the formation of co-current churn flow.

(B) At liquid rates below around 12 g/s, the downflow curve lies *above* the flooding curve. This result seems curious but can be explained if one recalls the definition of flooding used here, i.e. as the point at which liquid begins to be observed above the injector. The fact that liquid is carried above the injector does not mean necessarily that it then proceeds to leave the test section; it is likely that the so-called "hanging-film" phenomenon has been initiated above the injector in which a film exists with no net flow, downflow near the wall balancing upflow near the interface. Only when the liquid flowrate or air flowrate is increased to the downflow limit curve will net upflow of liquid begin. At this point, the transport of large waves may be possible and churn flow may occur.

The existence of these two regions is consistent with the qualitative observation of the nature of flooding reported above.

(3) The results for deflooding lie quite close to the downflow curve [as was found by Clift *et al.* (1966)] at high liquid flowrates but fall below it at low liquid flowrates. The deflooding curve lies below the flooding curve [consistent with the results of Wallis *et al.* (1963) and Hewitt & Wallis (1963)].

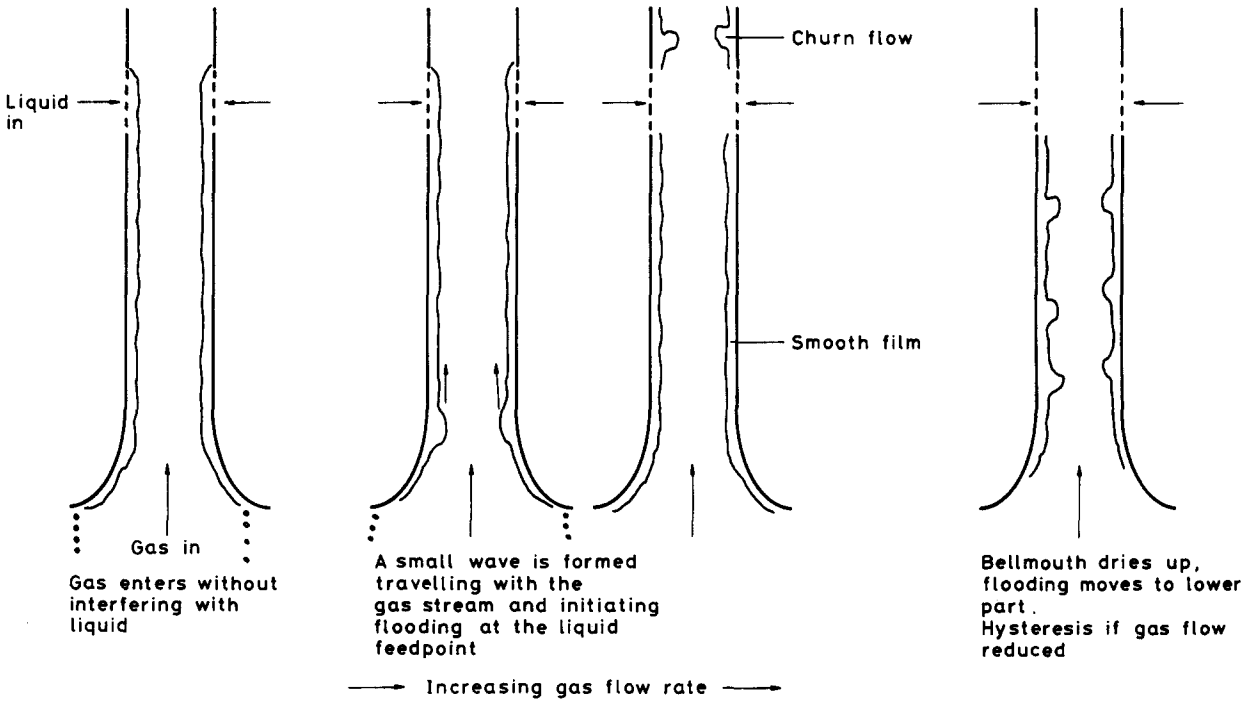

Figure. 7. The flooding mechanism in a test section with a tapered outlet.

2.2.2. Square and tapered outlets

For square and tapered outlets, the flooding and downflow curves become identical. Thus, in these experiments the air and water flowrates were set at values in the ranges 4–11 and 10–75 g/s, respectively (above the onset of flooding) and the liquid downflow rate was measured by timing the rise in the water level in the bottom part of the collection vessel.

The sequence of events in the test section with the tapered outlet is initially rather similar to that for the porous wall outlet, as shown in figure 7. However, as the gas flow is increased above flooding, there is a second point at which the gas interacts with the falling film to form a standing wave at the narrowest part of the taper. When this happens the liquid penetration is reduced and the pipe is filled with a churn-type flow. On reducing the gas flow the flow in the region below the injector reverts to a smooth falling film but some hysteresis was found, which is clearly shown in the results presented below.

In the test section with the square-edged outlet the sequence of events is different. In this case a rather thick standing wave forms at very low gas flowrates, as shown in figure 8. As the gas flow is increased some liquid is entrained from this wave but most of it redeposits on the falling film. Because the wave reduces the flow area for the gas, flooding takes place at lower gas flowrates than for the other test sections and appears always to occur at the *bottom* of the test section. In this case flooding occurs because, as the gas flow is increased, the rate at which water can escape from the bottom of the test section becomes less than the liquid input so the bottom part of the test section becomes filled with a churn-type flow which eventually reaches beyond the liquid injector. The flow behaviour in this case is very similar to the behaviour at high gas flows in the test section with the tapered outlet [figure 7(d)]. It was also observed that the water drains intermittently from the bottom of the test section, and this is accompanied by pressure fluctuations whose frequency depends on both the gas and liquid input flowrates. Thus, it was found that in this case the liquid penetration rate has a weak dependency on liquid input rate.

The penetration rate data for the square-edged and tapered outlets are shown in figure 9 and compared with the porous wall data. Figure 9 also shows the data of Hewitt (1977) for flooding in a 1.22 m test section ($\times$) and a 2.44 test section ($\bullet$) with square-edged outlets. The data for the square-edged outlet has considerable scatter, partly because of the dependency on liquid input flowrate discussed above, but is in good agreement with the flooding results of Hewitt (1977).

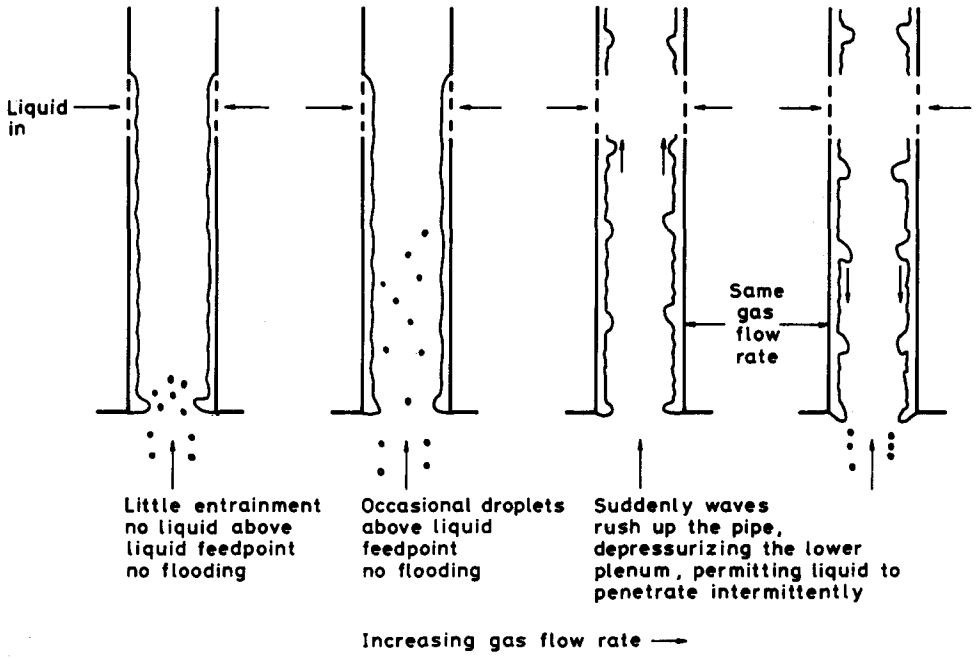

Figure 8. The flooding mechanism in a test section with a square-edged outlet.

The data for the tapered outlet is higher and shows the hysteresis at high gas velocities discussed above. Thus, as the gas flowrate is increased the liquid downflow rate decreases progressively until point A is reached. At this condition, as mentioned above, standing waves are formed at the outlet and downflow is initiated at the outlet and fills the whole tube. The liquid penetration rate decreases to a value commensurate with that for the square-edged outlet and is only reinstated to its previous value when the air flowrate is reduced to B.

The measurements using the porous wall outlet are also shown in figure 9 and lie well above the data for the square-edged and tapered outlets.

2.3. General Discussion

The new data in the paper has shown that there seem to be two extreme cases of flooding, namely that occurring in channels with smooth (porous wall) liquid outlets and fully developed, parallel gas inlet flow and, at the other extreme, sharp-edged liquid exit/gas entrance conditions.

For smooth entrance/exit conditions, the onset of flooding varies with tube length and can be initiated in two ways, namely by formation of a large liquid wave near the liquid outlet or by the spreading upwards of liquid interfacial disturbances with ultimate spread (but not transport) of the liquid above the injection. The visualization studies of McQuillan *et al.* (1985) illustrated the wave formation process, which is the dominant mechanism at higher liquid flowrates. Interfacial waves were observed on the surface of the liquid film but, prior to flooding, these moved downwards, through some of them grew rapidly as the flooding point was approached. At flooding, one of the waves is arrested, grows rapidly by accretion of other large waves falling into it and is then transported upwards and is carried beyond the liquid injection point, initiating the flooding process. There has been much controversy about the role of waves in the onset of flooding. Observations using continuous film thickness measurement and cross-correlation analysis have shown that, right up to flooding, the waves are in fact moving downwards. How, then, could waves moving upwards explain the flooding process? The answer is probably that the flooding process corresponds to the transport of only one wave and this unique event would not be picked up by the instrumentation used, for instance, by Zabaras & Dukler (1988). Once flooding has occurred, the large upward flowing waves can be repeatedly formed at the liquid injector since, instantaneously, the liquid flowrate is sufficient there as a result of drainage from the preceeding waves. The mechanisms of wave formation and transport in churn flow are discussed by Hewitt *et al.* (1985) and will be returned to below in the discussion of churn flow.

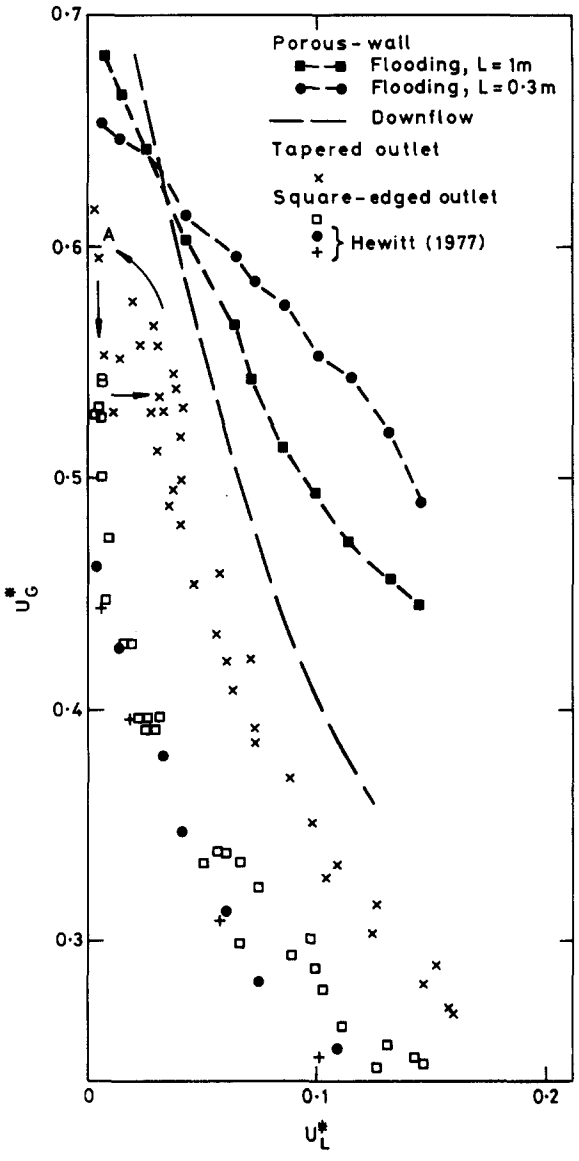

Figure 9. Effect of liquid outlet geometry on the flooding curve.

In the other extreme, we have the case of the sharp-edged liquid outlet/gas inlet where waves are formed associated with the gas phase vena contracta occurring at that point. The flooding rate for such a geometry is (as shown in figure 9) very much lower than that for a smooth liquid exit/gas inlet condition.

A number of authors (e.g. Zabaras & Dukler 1988) have used tapered liquid outlet conditions and this case falls between the two extreme cases, as illustrated in figure 9. In this case the downflow and flooding curves are coincident, which probably means that the wave formation mechanism is dominated by the liquid outlet configuration. However, the mechanisms seem similar to that for the smooth outlet, namely a single wave being suddenly formed near the liquid outlet and being swept upwards by the gas flow. However, the tapered outlet can exhibit the same kind of behaviour as the sharp-edged outlet at high gas flowrates, presumably due to separation occurring in the gas phase boundary layer and the formation of a vena contracta.

Undoubtedly, the most fundamental curve arising from the present measurement is that of downflow for the smooth liquid exit/gas inlet conditions. This is independent of the channel length and independent of the liquid inlet flow. The flooding curves can vary with channel length and, comparing the results of the present experiments with earlier ones with a similar geometry, are obviously quite sensitive to the precise experimental conditions. An analogy here would be the onset

of turbulence in pipe flow. If great care is exercised, then very high Reynolds numbers can be achieved before turbulence is initiated. However, very small disturbances are quickly amplified once the Reynolds number is in the turbulent region. A similar situation might occur with the wave formation mechanism clearly demonstrated in the case of smooth liquid outlet conditions.

3. CHURN FLOW EXPERIMENTS

As we have seen from section 2, co-current churn flow is initiated above the liquid injector following flooding, provided the liquid flow rate is >12 g/s. There is very little data on churn flow, particularly in circumstances where it co-exists with falling-film flow. Here, we report new data on the holdup and pressure drop for this region.

3.1. Apparatus and Measurement Methods

The apparatus had the same form as shown in figure 3 but used two slightly different configurations as follows:

Case 1 (with falling film). Here, the measurements were carried out in the post-flooded state and below the injector there was a falling film which was removed at the lower sinter. In this case the liquid flowrate in the churn flow regime was determined as the difference between the inlet flow and the measured downflow rate.

Case 2 (no falling film). In this case the outlet from the lower sinter is closed and the flow reaches a steady state in which the test section above the 10 mm restriction is filled with a churn-type flow. To investigate the effect of development length, a few measurements were also made in which the water was introduced at the lower sinter and the valve to the upper sinter was closed.

If the gas flow is above that for flow reversal (zero liquid penetration), cases 1 and 2 are identical. The region immediately above flow reversal is often described as churn–annular flow.

The holdup was measured using two valves which are mechanically linked and can therefore be closed simultaneously, the water contained in the section between the valves subsequently draining into a measuring cylinder. The valve bodies are machined from acrylic resin and are designed to be flush with the pipe inside wall when fully open. The valves were positioned with their centres 0.92 m apart and the total volume of the pipe section trapped between them when closed was measured as 0.725 ± 0.005 l. Further details of the design and testing of these valves are given by George (1975).

The pressure gradient was measured using two pressure tappings 846 mm apart connected across a differential pressure (DF) cell giving a voltage output. The trappings were kept free of air by "purging" them with water between readings. Due to the oscillatory nature of churn flow the DP cell output had large fluctuations; to obtain a mean value it was necessary to pass the output through an amplifier with a long time-constant (several seconds), which partially smoothed the fluctuations, then to a pen-recorder which enabled an estimate to be made of the mean pressure drop over times of around 3 min. The maximum uncertainty in the calculated pressure gradient is estimated to be around 60 N/m^3, dropping to around 15 N/m^3 in the churn–annular regime where the fluctuations are much smaller.

3.2. Experimental Data

Figures 10 and 11 show the measured pressure gradients and liquid holdup as a function of air mass flux in the region above the liquid injector after flooding has occurred. The criterion for flow reversal, $U_G^* = 1$, suggested by Wallis (1961), was found to be in good agreement with the present measurements and is represented by the vertical line in figures 10 and 11. For the points to the left of this line some of the input liquid flowed downwards as a falling film; the upflow rate is indicated by the figures adjacent to each point. For upward mass fluxes $\dot{m}_L$ of 47.7 and 31.8, respectively, curves were interpolated as shown representing the pressure gradients and holdup over the whole region. The error in this interpolation is estimated to be around 50 N/m^3 in the case of the pressure gradient (this is comparable to the experimental error) or around 0.005 in the case of the liquid holdup.

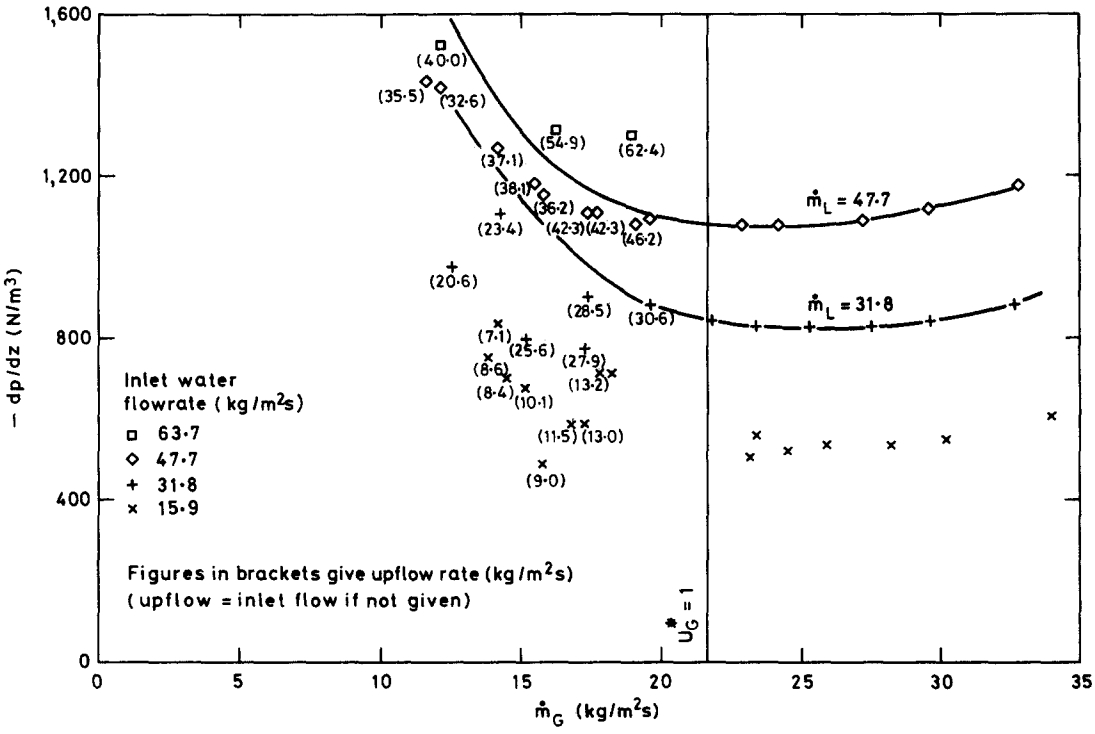

Figure 10. Measured pressure gradients in churn flow.

These interpolated curves for the pressure gradient and liquid holdup in the "post-flooding" state are reproduced in figure 12 and compared with similar data taken at the same flowrates when there was no falling film present. Figure 12 shows data taken with the upper sinter used as the liquid inlet and with the lower sinter used as the liquid inlet, as described in section 3.1. However, within the scatter of the data there is negligible difference between the measurements in the "post-flooding" state (i.e. with a falling film in the region below the injector) and those in churn flow

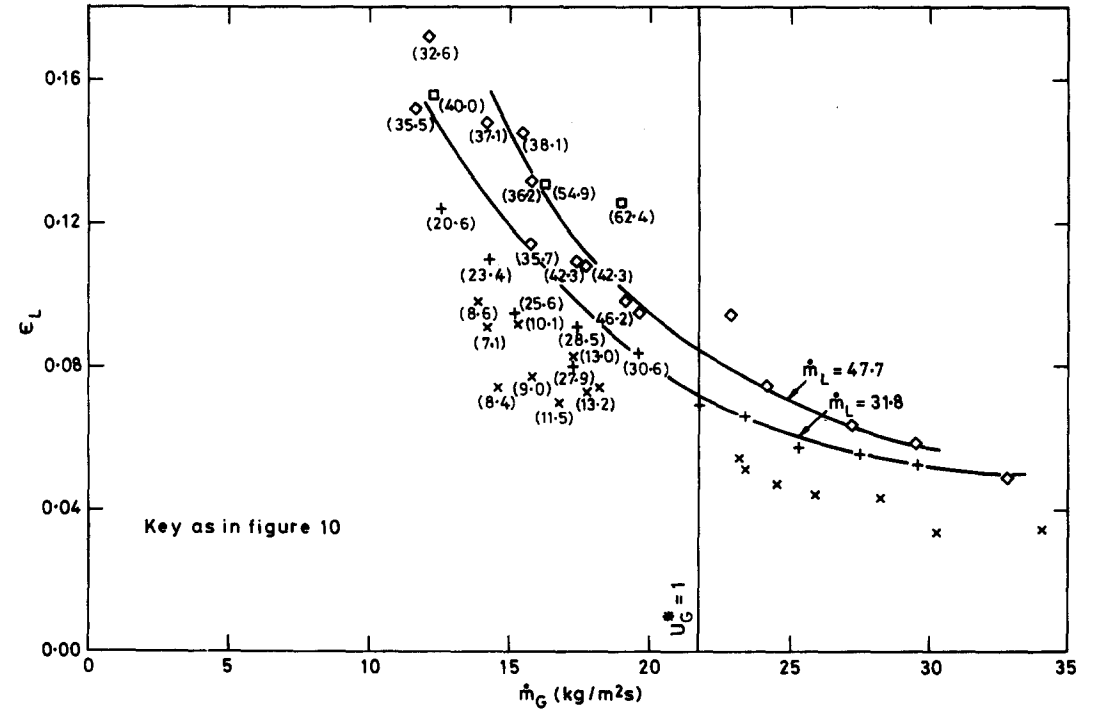

Figure 11. Measured liquid holdup in churn flow.

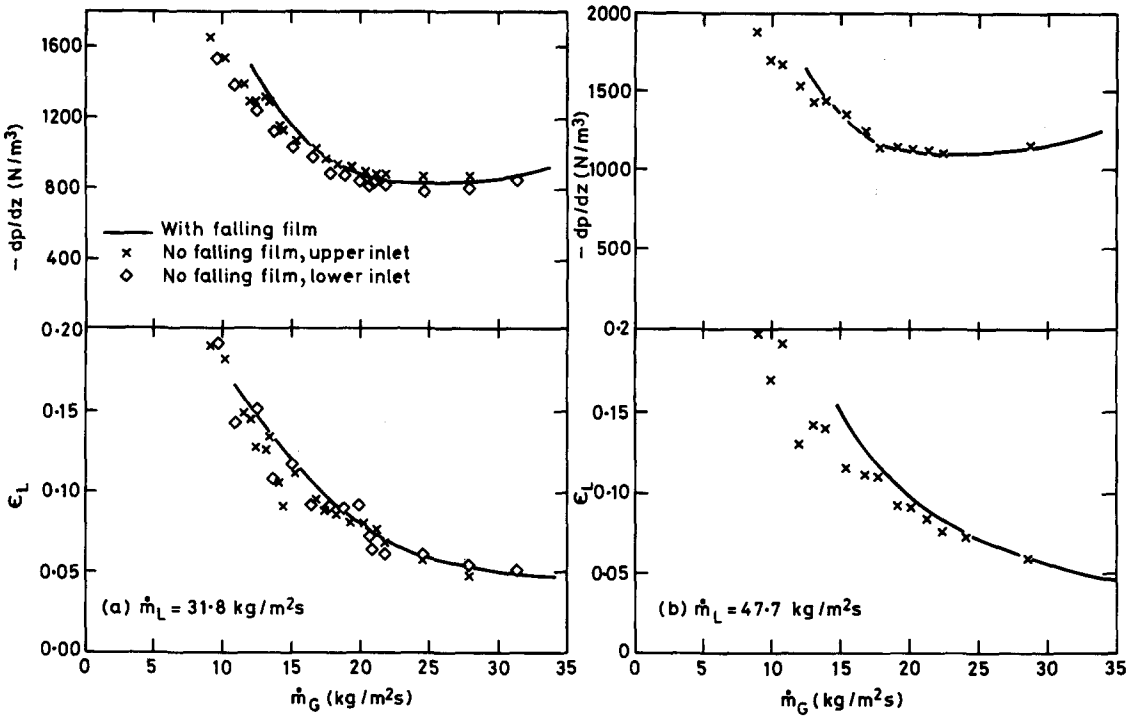

Figure 12. Comparison of the pressure gradient and holdup with and without a falling film.

(i.e. with no falling film). This confirms that, for practical purposes, the falling-film and churn flow regions existing beyond flooding are essentially decoupled.

3.3. Analysis of Churn Flow Data

The pressure gradient and holdup measurements may be used to calculate the mean wall shear stress, assuming negligible acceleration, from

$$-\frac{dp}{dz} = \frac{4\tau_0}{d} + \epsilon_L \rho_L g + \epsilon_G \rho_G g, \qquad [4]$$

where ϵ_L and ϵ_G are the liquid and gas holdup, τ_0 is the wall shear stress and dp/dz is the total pressure gradient. Typical results are shown in figure 13, where it may be seen that the condition of zero mean wall shear occurs at lower gas flowrates than the condition of minimum pressure drop. This is contrary to the calculations of Hewitt & Hall-Taylor (1970), using a laminar film model, who found that the two conditions were coincident at low liquid flowrates. Their results are shown in figure 14 in terms of the dimensionless parameters

$$\Delta p^* = \left(-\frac{dp}{dz}\right) \frac{1}{\rho_L g(1-\rho^*)}, \qquad [5]$$

$$K^* = \frac{g d^3 \rho_L^2 (1-\rho^*)}{8\eta_L^2} \qquad [6]$$

and

$$W^+ = \frac{\dot{M}_{LF}}{\pi d \eta_L}, \qquad [7]$$

where $\dot{M}_{LF}$ is the film flowrate, η_L is the liquid viscosity and $\rho^* = \rho_G/\rho_L$. The values obtained from the experimental data are also shown in figure 14, together with values obtained from the data of Hewitt *et al.* (1965), Willis (1965) and Hall-Taylor (1967). It is clear tht while the points representing the minimum pressure drop are in reasonable agreement with the laminar film model, the pressure gradients at the zero wall shear stress condition are significantly underpredicted. The reason for

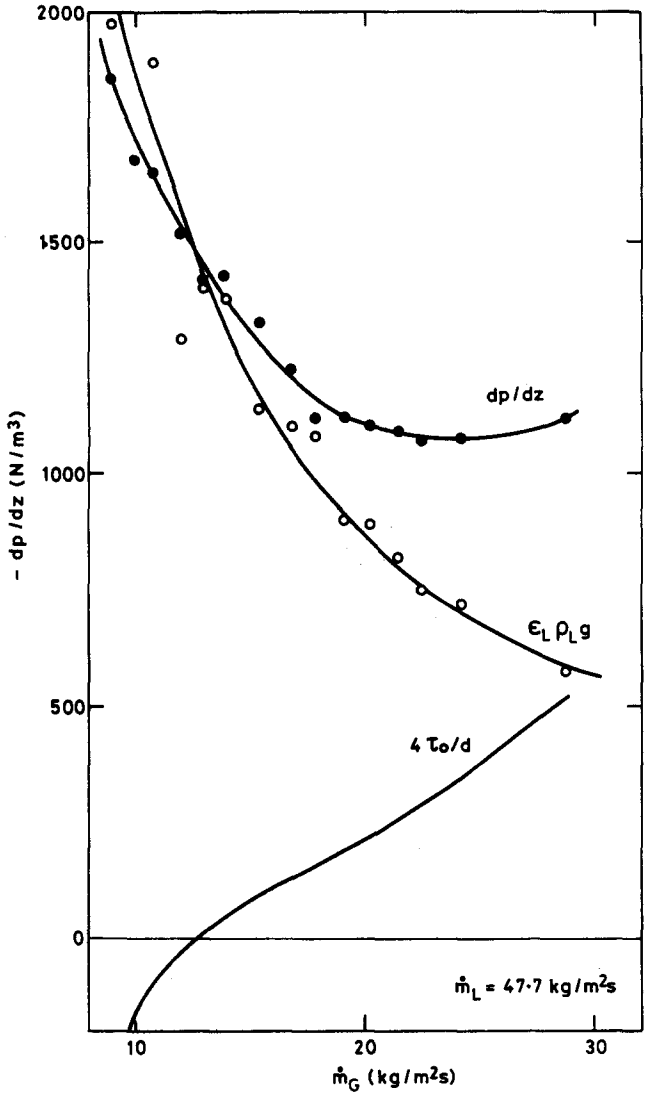

Figure 13. Wall shear stress calculated from pressure gradient and holdup data.

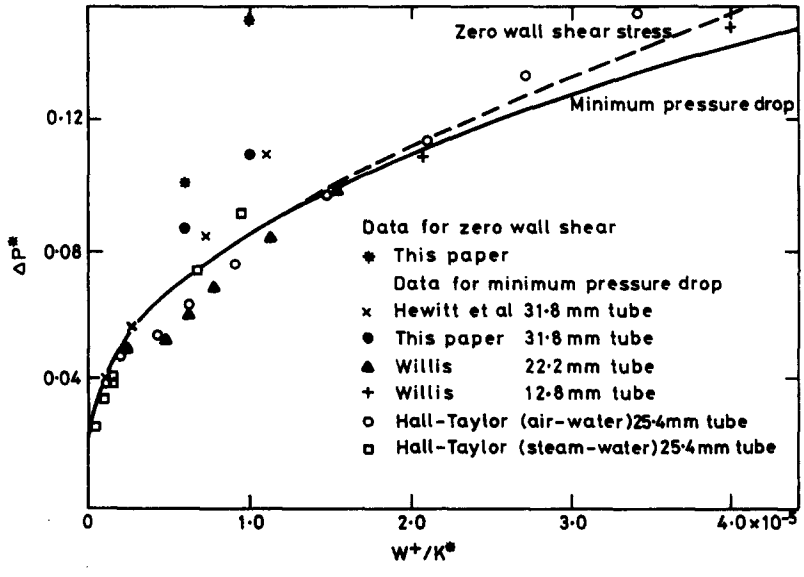

Figure 14. Dimensionless plot of zero wall shear and minimum pressure drop data.

the large discrepancy with the equations given above probably lies in the highly disturbed and turbulent nature of the flow which could hardly be expected to be described by a simple laminar theory.

From the point of view of nuclear safety calculations, it is interesting to compare the interfacial friction factor derived from these experiments with that used in reactor safety codes such as TRAC and RELAP. In these codes, an interfacial shear coefficient C_i is defined as follows:

$$C_i = \frac{F_{GL}}{(u_G - u_L)^2}, \quad [8]$$

where F_{GL} is the force (per unit volume) exerted on the liquid by the gas, and u_G and u_L are the gas and liquid velocities. Assuming that $u_G \gg u_L$, and putting

$$F_{GL} = \frac{\tau_i S_i}{A}, \quad [9]$$

where τ_i is the interfacial shear stress, S_i is the interfacial perimeter and A is the pipe cross-sectional area, gives

$$C_i = \frac{4\tau_i \epsilon_G^{0.5}}{du_G^2} = \frac{4\tau_i \epsilon_G^{2.5}}{du_G^2}. \quad [10]$$

The interfacial shear is calculated from the pressure gradient and liquid holdup data using the expression

$$\tau_i = \frac{r_i}{2}\left(-\frac{dp}{dz} - \rho_G g\right)$$

$$= \frac{d}{4}\sqrt{\epsilon_G}\left(-\frac{dp}{dz} - \rho_G g\right), \quad [11]$$

where r_i is the interfacial radius calculated on the assumption that all the liquid flows as a smooth film. Figure 15 shows the experimental data plotted as C_i vs ϵ_G.

In the RELAP5/MOD2 code there is no provision for churn flow in the flow pattern map; the slug/annular transition takes place at a void fraction given by

$$\epsilon_{GT} = \max\left\{0.75, 1.4\frac{[\sigma g(\rho_L - \rho_G]^{0.25}}{u_G \rho_G^{0.5}}\right\}, \quad [12]$$

where σ is the surface tension. Using this criterion all but two of the points in figure 15 are in annular flow. The TRAC-PF1/MOD1 code, on the other hand, has the slug/churn transition at a voidage of 0.5 and the churn/annular transition at a voidage of 0.75, so with this criterion all the points are in annular flow. In the RELAP5 code C_i is calculated from [10], with τ_i given by

$$\tau_i = \tfrac{1}{2} f_i \rho_G u_G^2, \quad [13]$$

where f_i is given by a form of the equation of Bharathan *et al.* (1978), which reduces to

$$f_i = 0.005 + 14.44\epsilon_L^{2.03} \quad [14]$$

for the experiments described here. In the TRAC code it is assumed that $S_i \approx \pi d$, in which case [10] becomes

$$C_i' = \frac{4\tau_i}{du_G^2}, \quad [15]$$

where τ_i is calculated using [13] and the Wallis (1969) correlation for f_i:

$$f_i = 0.005(1 + 75\epsilon_L). \quad [16]$$

The values of C_i calculated using [14] and [16] are shown in figure 15 (using [10] in both cases, for consistency), where it can be seen that the Wallis correlation only gives good results for $\epsilon_G \gtrsim 0.95$, while the Bharathan equation gives reasonable results over most of the range. This is not surprising

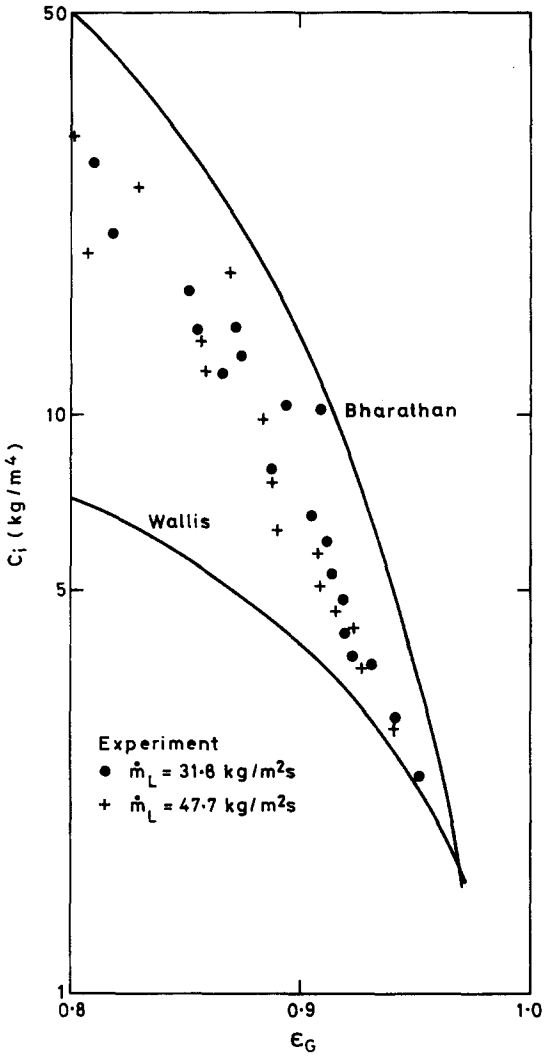

Figure 15. Comparison of the calculated and predicted interfacial shear coefficient.

since the Wallis correlation was derived for fully developed annular flow and the Bharathan correlation was derived for (effectively) churn flow conditions similar to the ones in the present experiment.

4. CONCLUSIONS

From the experiment described in this paper, it is concluded that:

(1) For test sections with smooth liquid outlet/gas inlet conditions, the onset of flooding (defined as the transport of liquid beyond the injection point) is significantly affected by the channel length, in agreement with previous data for similar geometries. However, the rate of liquid penetration beyond flooding is independent of channel length, as the new data here show for the first time for this geometry. The flooding and downflow (penetration) curves cross over one another as the liquid flowrate is reduced and the gas flowrate increased. At high liquid flowrates, the onset of flooding corresponds to the formation and transport of a single wave near the liquid outlet. This initiates the churn flow regime above the injector. At low liquid flowrates, liquid is transported above the injector but forms a hanging film there and there is no net upwards flow in the region between the flooding and downflow curves. Once the liquid flowrate is increased beyond the downflow curve, then net liquid transport upwards begins even in this region.

(2) In the test section with a square-edged liquid outlet/gas inlet, the flooding rate was drastically lower than that found for smooth entrance conditions. This reflects the fact that the flooding process appears to be governed by a vena contracta at the gas entrance, explaining the fact that flooding in such geometries is independent of the falling-film length.
(3) For a tapered or bell-mouth liquid outlet/gas inlet, the flooding and downflow curves are coincident, as also found by Zabaras & Dukler (1988), but both lie below the values for the smooth-end conditions. Normally, flooding is initiated in this situation by the formation of a single wave near the liquid outlet but, clearly, the outlet conditions have influenced the formation of the wave, giving rise to lower flooding rates. There is some evidence that gas boundary layer separation will occur at high enough gas rates leading to similar results to those for the sharp-edged liquid outlet/gas inlet.
(4) Measurements have been made of the co-current churn flow region occurring after flooding above the liquid injection point. Measurements on churn flows with and without a co-existing liquid film show that these are essentially identical in behaviour (as manifested by identical pressure gradients and liquid holdup) and this shows that beyond flooding, the churn flow region above the injector and the falling film region below the injector are essentially decoupled.
(5) Calculation of mean wall shear stress from the pressure gradient and holdup measurements in churn flow showed that the condition of zero wall shear stress occurred at a somewhat lower gas velocity than that for the minimum pressure gradient. The laminar flow analysis summarized by Hewitt & Hall-Taylor (1970) indicated that the zero wall shear stress and minimum pressure drop conditions were similar but, in reality, it is doubtful whether the film behaviour could be described by such a simplified analysis. It may be possible to develop a more complex, turbulent flow, analysis though the boundary conditions are particularly challenging.
(6) An important application of data on two-phase flow is within the context of nuclear reactor safety codes and the present data has been compared to the current models within the two principal codes, namely TRAC and RELAP. For the present results for churn flow, the method used in RELAP (Bharathan *et al.* 1978) would appear to be better than that used in TRAC (Wallis 1969).

Acknowledgements—This work was undertaken as part of the Underlying Research Programme of the UKAEA. The authors wish to thank Peter Lovegrove and Peter Stepney (Harwell Laboratory) for their help with the construction of the rigs and also David Benn (formerly Harwell Laboratory) for his help with the instrumentation.

REFERENCES

BANKOFF, S. G. & LEE, S. C. 1986 A critical review of the flooding literature. In *Multiphase Science and Technology*, Chap. 2 (Edited by HEWITT, G. F., DELHAYE, J. M. & ZUBER, N.). Hemisphere, New York.

BHARATHAN, D., RICHTER, H. J. & WALLIS, G. B. 1978 Air–water counter-current annular flow in vertical tubes. Report EPBI-NP-786.

CLIFT, R., PRITCHARD, C. L. & NEDDERMAN, R. M. 1966 The effect of viscosity on the flooding conditions in wetted wall columns. *Chem. Engng Sci.* **21,** 87–95.

FEIND, F. 1960 Falling liquid films with counter-current air flow in vertical tubes. *VDI Forsch.* 481.

GEORGE, K. 1975 Measurement of liquid holdup for air–water mixtures flowing upwards in a vertical tube. Report AERE-M2420.

HALL-TAYLOR, N. S. 1967 Interfacial wave phenomena in vertical annular two-phase flow. Ph.D. Thesis, Univ. of Cambridge, Cambs.

HEWITT, G. F. 1977 Influence of end conditions, tube inclination and physical properties on flooding in gas–liquid flows. Report HTFS RS222.

HEWITT, G. F. 1989 Countercurrent two-phase flow. In *Proc. NURETH-4 (4th Int. Top. Mtg on Nuclear Reactor Thermal Hydraulics).* Vol. 2.

HEWITT, G. F. & HALL-TAYLOR, N. S. 1970 *Annular Two-phase Flow.* Pergamon Press, Oxford.

HEWITT, G. F. & WALLIS, G. B. 1963 Flooding and associated phenomena in falling film flow in a vertical tube. Report AERE-R4022.

HEWITT, G. F., LACEY, P. M. C. & NICHOLLS, B. 1965 Transitions in film flow in a vertical tube. Report AERE-R4614. Also presented at the *Symp. on Two-phase Flow*, Exeter, Devon, Paper B4.

HEWITT, G. F., MARTIN, C. J. & WILKES, N. S. 1985 Experimental and modelling studies of annular flow in the region between flow reversal and the pressure drop minimum. *Physicochem. Hydrodynam.* **6,** 69–86.

MCQUILLAN, K. W. 1985 Flooding in annular two-phase flow. Ph.D. Thesis. [See also: WHALLEY, P. B. & MCQUILLAN, K. W. 1985 Flooding in two-phase flow: the effect of tube length and artificial wave injection. *Physicochem. Hydrodynam.* **6,** 3–21.]

MCQUILLAN, K. W., WHALLEY, P. B. & HEWITT, G. F. 1985 Flooding in vertical two-phase flow. *Int. J. Multiphase Flow* **11,** 741–760.

WALLIS, G. B. 1961 Flooding velocities for air and water in vertical tubes. Report AEEW-R123.

WALLIS, G. B. 1969 *One-dimensional Two-phase Flow*. McGraw-Hill, New York.

WALLIS, G. B., STEEN, D. A. & BRENNER, S. N. 1963 AEC Report NYO-10487 EURAEC 890.

WILLIS, I. J. 1965 Upwards annular two-phase air–water flow in vertical tubes. *Chem. Engng Sci.* **20,** 285.

ZABARAS, G. J. & DUKLER, A. E. 1988 Counter-current gas–liquid annular flow including the flooding state. *AIChE Jl* **34,** 389–396.